B. Witschas 24.01.2022

The valuable comments given by the anonymous Referee #2 (received on 15 January 2022, shown in black) are highly appreciated. The corresponding answers of the authors, indicated in blue color, as well as the related changes in the manuscript, indicated in green color, are given below.

Interactive comment on "Spectral performance analysis of the Aeolus Fabry-Pérot and Fizeau interferometers during the first years of operation" by B. Witschas et al.

(Reviewer comments) (Author response) (changes in the manuscript)

1. The optical frequency discrimination performance of Doppler lidar seriously affects the accuracy of wind speed measurement. This paper does not mention how the frequency discrimination performance affects the measurement accuracy with the system operation.

This question is rather complex to answer, as a lot of steps are performed in the Aeolus processor to derive HLOS winds. Thus, it is difficult or rather impossible to relate any FPI alignment drifts directly to a systematic error of the derived wind speed. Hence, also a forward modelling of the induced systematic error is out of scope for this publication, as much more detailed information about the wind processing and corresponding calibration procedures have to be addressed in advance. In particular, there is only one step in the processing chain where the FPI transmission curve fits are used, namely the so-called Rayleigh-Brillouin correction (Dabas et al., 2008, Dabas and Huber, 2017), where the impact of temperature and pressure differences in various altitudes on the receiver response is considered. To perform this correction, the fits are convolved with Rayleigh-Brillouin spectra that are calculated for different temperatures and pressures, and the derived response change is used for correction. However, as the atmospheric channel has different optical properties than the internal reference channel, further modifications have to be performed. In particular, the fits of the internal reference FPI transmission curves are convolved with a tilted top-hat function to consider any optical etendue effects, which considers the different optical illuminations of the atmospheric and reference channel. The accuracy of this procedure cannot be well assessed, as there is no possibility to measure the FPI transmission curves via the atmospheric channel with the needed accuracy. Among others, this is the reason why additional bias corrections based on ground return or ECMWF-model data are performed to obtain a wind product with a small systematic error of e.g. < 1 m/s. This bias correction is extensively explained by Weiler et al., 2021. Furthermore, as the width (FWHM) of the Rayleigh-Brillouin spectrum is rather broad (i.e. about 3 to 4 GHz for a laser wavelength of 355 nm and atmospheric pressures from 0 hPa to 1013 hPa and temperatures from 220 K to 330 K), the response of the Rayleigh channel is insensitive to small scale details as observed for the FPI transmission curve residuals. In order to clarify this issue, we add the following explanations to the manuscript: Following line 358: "It is also worth mentioning here, that the shown deviations cannot directly be related to a potential systematic error, as several steps are performed during the wind processing chain. The only processing step that directly applies FPI transmission fit curves is the RBC that considers the impact of different atmospheric temperatures and pressures on the receiver response (Dabas et al., 2008; Dabas and Huber, 2017). Within the RBC, the FPI fit curves are convolved with Rayleigh-Brillouin spectra of different temperatures and pressures, as well as with a tilted top-hat function to consider the different optical illumination between the internal reference and the atmospheric path. The particular accuracy of the latter procedure cannot be well assed, as there is no possibility to measure the FPI transmission curves via the atmospheric path with the needed accuracy. Among others, this is the reason why additional bias corrections based on ground return signals or ECMWF-model data are performed to obtain a wind product with a small systematic error of below e.g. ≈ 1 m/s. This bias correction

is extensively explained by Weiler et al. (2021b). Additionally, as the width of the RB spectrum is rather broad (i.e. 3 to 4 GHz for a laser wavelength of 355 nm and atmospheric temperatures and pressures), the response of the Rayleigh channel is insensitive to small scale details as observed for the FPI transmission curve residuals.". Furthermore, the following references were added:

- Dabas, A. and Huber, D.: Generation and update of AUX CSR, AE.TN.MFG-L2P-CAL-003, p. 43, https://earth.esa.int/eogateway/news/announcement-of-opportunity-for-aeolus-cal-val, 2017
- Rennie, M., Tan, D., Andersson, E., Poli, P., Dabas, A., De Kloe, J., Marseille, G.-J., and Stoffelen, A.: Aeolus Level-2B Algorithm Theoretical Basis Document (Mathematical Description of the Aeolus Level-2B Processor), ECMWF, https://earth.esa.int/eogateway/documents/20142/37627/Aeolus-L2B-Algorithm-ATBD.pdf, 2020.

2. This paper mentioned that the frequency discrimination performance of Doppler lidar is mainly caused by the alignment stability and the laser quality. In my experience, the performance of the detector also affects the efficiency of photoelectric conversion, especially for ACCD.

It is agreed that the quantum efficiency of the detector affects the overall signal level and with that the magnitude of the random error. However, regarding the instrumental alignment and the spectrometer performance, the ACCD detectors play a minor or even negligible role. The quantum efficiency of the ACCD detectors was characterized to be 85% (Reitebuch et al., 2009, Weiler et al., 2021), and there are no measurements available that indicate any change of the quantum efficiency during the mission lift-time. An issue that was identified quite at the beginning of the mission but not during ground tests was, that the ACCD detectors suffer from an increasing number of hot-pixels that arise during life time and that can induce a systematic error in the retrieved wind speeds. Thus, a special measurement mode as well as a corresponding correction procedure was developed as described by Weiler et al., 2021a (see also line 37). However, these hot-pixels arise only in the memory zone of the detector and thus, do not affect ISR measurements with the internal reference signal.

3. Why don't chose PMT detectors in this system, and apply FPI for Doppler frequency discrimination of Mie doppler signals?

Although the original system specifications are not in the scope of this paper, it is tried to explain the reasons why the actual Aeolus spectrometers and detectors were chosen with the current specifications. Since the spectral widths of the molecular backscattered light (FWHM ~ 3-4 GHz) and the light backscattered on particles (FWHM ~0.05 GHz) differ by almost 2 orders of magnitude, different spectrometers with different bandwidths have to be used for frequency discrimination.

For the Mie channel, it was decided to use a Fizeau interferometer in fringe-imaging configuration to analyze the narrowband return of particulate scattered light. Using a Fizeau interferometer is beneficial here, as the formed interference pattern is a "straight" line (fringe) that can easily be imaged onto a 2D-detector and can be analyzed more easily compared to the circular interference pattern that would originate from an FPI. In addition, the ACCD is able to accumulate returns from successive laser pulses directly on the chip in an internal accumulation register. Thus, the summation of pulse returns does not need a reading of each one of them, which would lead to additional readout noise.

For the Rayleigh channel, it was decided to use the common and approved double-edge technique. To prevent any additional efforts with additional space-qualification procedures of additional detectors (e.g. PMTs), it was decided to use the same ACCD detector for both channels. Furthermore, the ACCDs provide a rather good quantum efficiency of 85% at ultraviolet wavelengths, and low dark current and read-out noise, which allows quasi-photon counting. In addition, having a 2D ACCD detector for the Rayleigh channel gives further opportunities to analyze the system performance. For instance, the Rayleigh spot position behind/after the FPIs provides further information on the system alignment and potentially ongoing drifts.

4. How to normalize the long-term FPI transmission curves, in the line 380 and why the direct channel normalization forms of Fig. 5(a) and Fig. 5(b) are inconsistent?

The direct channel transmission curves are normalized to unit area, and the reflected channel is scaled with the same value as the direct channel in order to keep the ratio between the two transmission curves. Furthermore, the x-axis is normalized to the direct channel center frequency, whereas the center frequency is chosen from the fit. The normalization of the direct channel transmission curves for the FM-A period (Fig. 5, a) and FM-B period (Fig. 5, b) is consistent but looks different. This has mainly to do with the changing modulations that are caused by the reflection on the Fizeau interferometer and a changing laser beam profile. These modulations were larger for the FM-B period (e.g. at +1.0 GHz) and lead to varying peak intensity levels when the normalization is performed to unit area. To clarify the normalization, the following explanation was added: "To be able to directly compare respective measurements, the direct channel transmission curves are normalized to unit area such that $\int_0^{\mathcal{F}_{\mathrm{FSR}}} \mathcal{T}_{\mathrm{dir}}(f)\,df = 1$, and the reflected channel is normalized accordingly with the same factor as used for the direct channel to keep the ratio between the two respective channels.".

5. The beam divergence angle of the incident FPI has a serious impact on the transmittance of the FPI in line 570. The larger divergence angle corresponds to the greater FWHM and the lower transmittance of the FPI. According to the optical path setting in Fig. 1, only one collimating mirror is used to collimate the received signal light. The signal light is reflected by the Fizeau interferometer and then enters the direct channel of the FPI. The reflected light of the direct channel enters the reflection channel of the FPI, and the optical path is too long. How to ensure the incident FPI with minimal divergence angle.

In line 83 of the original manuscript, we provide the following information: "Furthermore, the transmit-receive optics contain a field stop (FS) with a diameter of about 88 µm in order to set the field of view (FOV) of the receiver to be only 18 µrad which is needed to limit the influence of the solar background radiation and the incidence angle on the spectrometers.". Thus, the instrument field of view and the spectrometer divergence is basically determined by the size of the filed stop. As the input beam diameter changes for the Fizeau interferometer and the FPIs, and as the étendue is preserved, the spectrometers are illuminated with a different divergence, but the divergence is the same for the direct channel and the reflected channel FPI. In principle, the divergence on the spectrometers could be further reduced by minimizing the size of the field stop or increasing the beam size and aperture of the interferometer. However, this would require a further reduced laser beam divergence to avoid clipping and lead to higher costs. Furthermore, the system would be more sensitive to alignment changes in case of an even smaller field stop size.

6. In line 135, 20 laser pulses for each measurement are used, while 190 pulses is used in 145 line, please explain it clearly.

During an ISR measurement, three different frequency steps are performed per observation, and each observation consist of 30 measurements with 19 laser pulses. Thus, one frequency step lasts for 10 measurements and contains the data of 190 laser pulses. To clarify this issue, the following sentence was added or rather extended: Following line 139: "…83790 laser pulses, and each measurement at a certain frequency step consists of 10 measurements and contains the data of 190 laser pulses" Additionally, we mentioned in line 138 that every last laser pulse of a measurement does not contribute to the accumulated signal, thus using only 19 out of 20 pulses.

7. Lines 155-190 describe the process of laser energy drift correction. For the reader's convenience, a simple system schematic diagram including optical and electrical devices is recommended.

It is agreed that the applied laser energy drift correction was not explained sufficiently in the original manuscript. To further clarify, we added an additional figure and a paragraph: Following line 189: "… factor that is derived by the analysis of FPI transmission curve residuals such that the residual exhibits no skewness anymore. This procedure is illustrated in Fig. 3, where panel (a) shows the laser energy measured by PD-74 and normalized to the first data point $E_{norm}(f)$ (blue) as well as the corrected normalized laser energy $E_{normnew}(f)$ (orange) for the ISR measurement performed on 10 October 2018. In panel (b), the respective FPI transmission curves of the direct channel, derived by using $E_{norm}(f)$ (blue) and $E_{normnew}(f)$ (orange) for the laser energy drift correction are shown. The corresponding relative residuals are shown in panel (c). The line fits applied to the data reveals that the slope is close to zero, when $E_{normnew}(f)$ is used for the laser energy correction (orange), whereas a significant skewness is obvious when Enorm(f) is used (blue). It can be seen that the relative deviations vary between -2% and 4% (peak-to-peak), whereas the distinct modulation is caused by an insufficient description of the spectral features of the Fizeau reflection and modulations of the incident laser beam profile and/or the transmission over the Fizeau aperture (see also Fig. 4 and the corresponding discussion). For the ISR measurement on 10 October 2018, ξ_i was determined to be 0.04. For the entire mission time discussed in this paper (October 2018 until March~2021), ξ_i varies between 0.05 and -0.18. ".

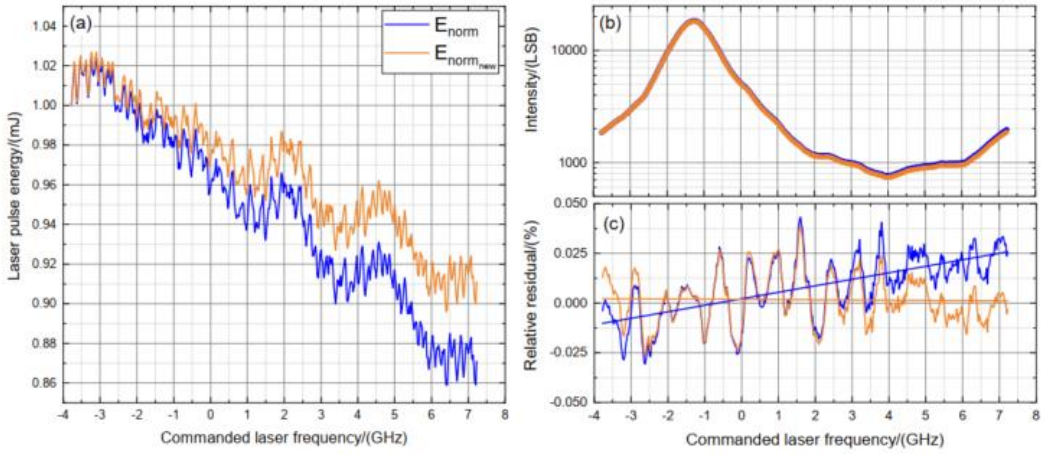

Figure 3. (a): Normalized laser energy $E_{\mathrm{norm}}(f)$ (blue) and corrected normalized energy $E_{\mathrm{norm}_{\mathrm{new}}}(f)$ (orange) versus commanded laser frequency for the ISR measurement performed on 10 October 2018. (b): Corresponding FPI transmission curves of the direct channel according to Eq. (2) by using $E_{\mathrm{norm}}(f)$ (blue dots) or rather $E_{\mathrm{norm}_{\mathrm{new}}}(f)$ (orange dots) for the laser energy drift correction. To illustrate the small differences, the y-axes is plotted with logarithmic scale. (c): Relative residuals of the best fits according to Eq. (9) and line-fits.